GLAs (H, number of subclones = 64) again display a prevalence of BG over GLAs (mean ratio = 1.310, 0.270 log units, $P = 0.017$). Number of bins = 10. In each plot, the vertical solid line indicates 1:1 ratio, the vertical dotted line indicates the mean ratio, and the light-colored area indicates the 95% bootstrap confidence interval of the mean. *P* values are computed with Wilcoxon signed rank test against zero. The numerical data used in panels (A,E,F,G,H) are included in S1 Data. A-P, antero-posterior; BG, Bergmann glia; D-V, dorso-ventral; GLA, granular layer astrocyte; HetC, heterogeneous clone; M-L, medio-lateral; NND, Nearest Neighbor Distance; PCL, Purkinje cell layer; WM, white matter; WMA, white matter astrocyte.

https://doi.org/10.1371/journal.pbio.2005513.g005

Specific features and different fates of clones emerge postnatally

To elucidate the dynamics of clone allocation and amplification, we analyzed clones at birth (P0, Fig 6A). Similar to P30, E12-targeted cells were, for the most part, settled laterally, whereas E14-P0 clones were preferentially located medially (Fig 6B). Likewise, the A-P distribution of P0 clones essentially resembled that observed at P30 (Fig 6B).

All tested StarTrack-labeled cells displayed positivity for brain lipid–binding protein (BLBP), which marks astroglial precursors or negativity for the interneuron progenitors transcription factor paired box gene 2 (PAX2), or for the oligodendroglial lineage marker SRY-box 10 (SOX10) [15,18] (S6 Fig and Methods). Moreover, cells in the prospective white matter (PWM) expressed nuclear factor 1 A (NFIA), which labels astrocyte progenitors [19] (S6 Fig). Taken together, these data confirm that the tagged cells are astrocyte progenitors.

Most cells formed HomCs in the PWM (Fig 6C), including elements with the typical fibrous shape of WMAs and cells with a basal process extending from the soma towards the pial surface (Fig 6A'). These latter resembled RG detached from the VZ, formerly proposed as a source of BG [10]. A minor proportion of cells formed clones still at the VZ. About 30%–40% of clones (Fig 6C) were also found in the nascent cortex, where cells already displayed morphologies distinctive of bona fide radial BG precursors settled in the PCL (PCL precursors [PCLps]) or stellate GLA precursors (GLAps, Fig 6A"). HetCs were still rare and included a very small fraction of PCLp+GLAp clones, or cortical+PWM clones (Fig 6C).

At difference with P30 data, the average size of both E12-P0 and E14-P0 clones was still rather small (3.7 versus 3.2 cells/clone, respectively; Fig 6D). However, consistent with P30 results, HetCs already contained more cells than HomCs (Fig 6D). Similarly, HetCs tended to be more dispersed mediolaterally compared to HomCs (Fig 6E). However, E12-P0 and E14-P0 M-L dispersions did not differ yet (Fig 6E). Altogether, these results show that, at birth, layer allocation, size, and degree of dispersion are not yet achieved, whereas the positional choice of clones along the cerebellar axes is already defined.

In support of this view, comparison of P0 and P30 data showed that HetCs proportionally increased with time in the whole clone population for both E12- and E14-derived cells (Fig 6F). Interestingly, this correlated with a reduction of E12 PWM HomCs by half (Fig 6F), suggesting that the P0 hemisphere PWM still hosts a number of MPs capable of producing HetCs. Moreover, the fraction of P0 PCLp HomCs significantly decreased compared to P30 data for both E12- and E14-derived lineages (Fig 6F). Therefore, PCLp in both hemispheres and vermis may generate different astrocyte types.

PCLps are the source of distinct astroglial types after birth

To clarify whether PCLps generate different astrocyte types, we employed $R26R^{Confetti}$ reporter mice [20] that enable the distinction of progenies derived from individual progenitors through stochastic and exclusive expression of 1 out of 4 fluorochromes. To induce recombination in PCLps, we applied tamoxifen (Tx) on the cerebellar surface [15] (Fig 7A) of $GLAST^{CreERT2/+}$ x$R26R^{Confetti/+}$ (Confetti) mice at P6, when only progenitors in the PCL own a basal process. We adopted a protocol that allowed targeting of a limited number of PCLps to follow the

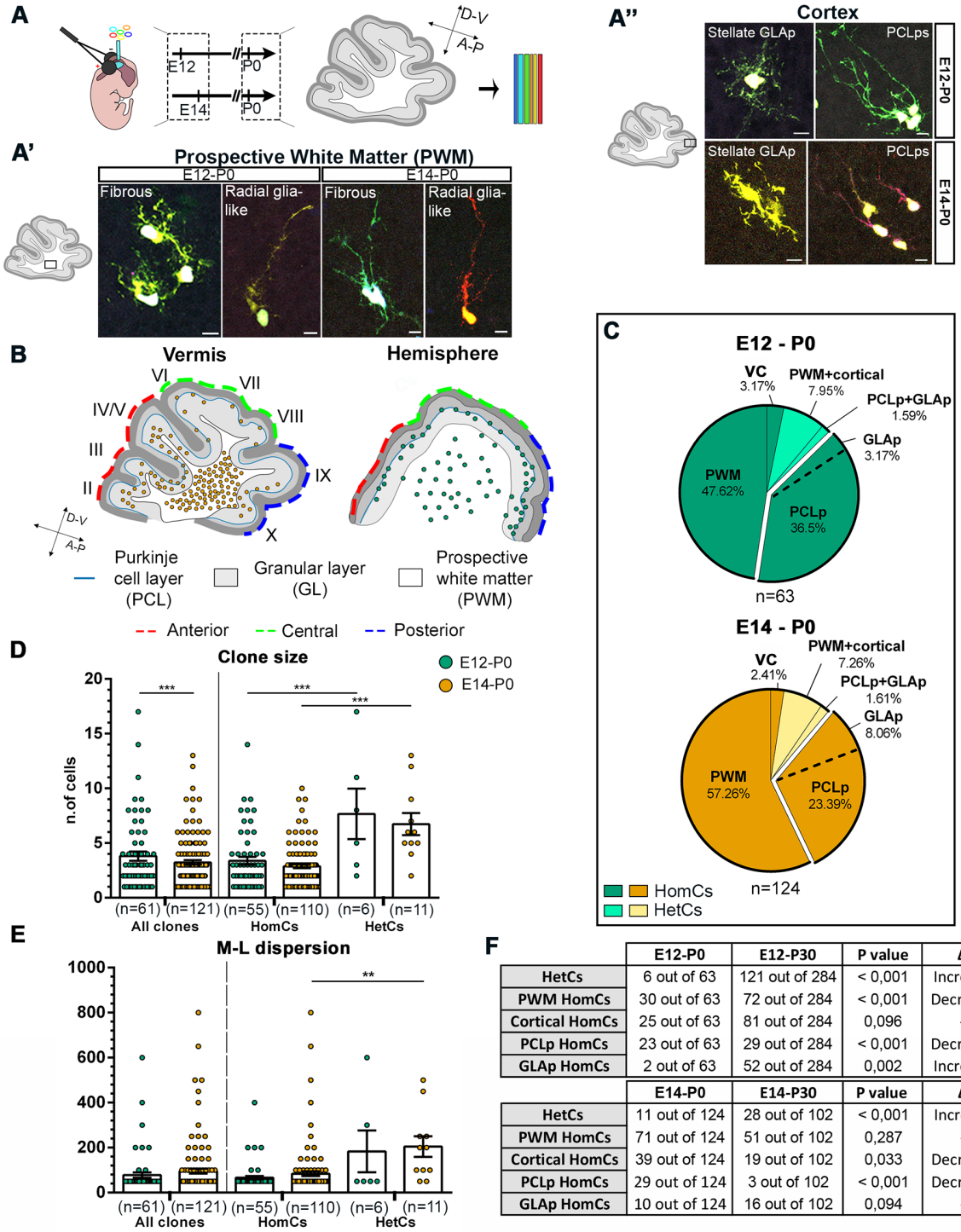

F

	E12-P0	E12-P30	P value	Δ
HetCs	6 out of 63	121 out of 284	< 0,001	Increase
PWM HomCs	30 out of 63	72 out of 284	< 0,001	Decrease
Cortical HomCs	25 out of 63	81 out of 284	0,096	-
PCLp HomCs	23 out of 63	29 out of 284	< 0,001	Decrease
GLAp HomCs	2 out of 63	52 out of 284	0,002	Increase

	E14-P0	E14-P30	P value	Δ
HetCs	11 out of 124	28 out of 102	< 0,001	Increase
PWM HomCs	71 out of 124	51 out of 102	0,287	-
Cortical HomCs	39 out of 124	19 out of 102	0,033	Decrease
PCLp HomCs	29 out of 124	3 out of 102	< 0,001	Decrease
GLAp HomCs	10 out of 124	16 out of 102	0,094	-

Fig 6. Analyses of clones at birth. (A) Schematic representation of the experimental design. IUE of the hGFAP-StarTrack mixture was performed at E12 or E14 and clonal analysis at P0. Representative examples of tagged cells at P0 comprising fibrous cells and RG-like cells in the PWM (A'), stellate GLA (GLAp), and PCLps of BG in the developing cortex (A''). (B) Schematic representation of clone distribution along the A-P and M-L axes. Early clones tagged at E12 (green) are settled in the hemispheres and are homogeneously distributed in all the developing lobules. Clones tagged at E14 (orange) are found in the vermis and allocate preferentially to anterior and, less frequently, to posterior lobules. (C) After both E12 and E14 IUE, HomCs are mostly found in the PWM at P0. A relevant proportion is also found in cortical layers ("exploded" sections), mostly as clones composed of PCLps. HetCs are still rare and include clones with cells in the two developing cortical layers (PCLp +GLAp) or in both PWM and cortex (PWM+cortical, comprising BGp+PWM, GLAp+PWM, and BGp+GLAp+PWM clones). Pies illustrate pooled data from 3 animals per time point. (D) Scatterplots show the size of E12 (green) and E14 (orange) clones at P0. Early- and late-tagged

clones show statistically different sizes, despite the difference being negligible. At both time points, HomCs are smaller than HetCs. (E) Scatterplots show the M-L dispersion of E12- and E14-derived clones at P0. E12 and E14 clones do not differ in their M-L dispersion ($P = 0.502$). HetCs at both time points tend to be more dispersed than HomCs. (**, $P < 0.01$; ***, $P < 0.001$; *P* values are calculated with GEE analysis). Table in (F) summarizes the numbers of clones in each layer at P0 and P30 and the *P* values resulting from their comparisons by Fisher's exact test. *n* = number of clones. Scale bars: 10 μm. The numerical data used in panels (D,E) are included in S1 Data. A-P, antero-posterior; D-V, dorso-ventral; E, embryonic day; GEE, generalized estimating equations; GL, granular layer; GLAp, granular layer astrocyte precursor; HetC, heterogeneous clone; hGFAP, human glial fibrillary acidic protein; HomC, homogeneous clone; IUE, in utero electroporation; M-L, medio-lateral; P, postnatal day; PCL, Purkinje cell layer; PCLp, Purkinje cell layer precursor; PWM, prospective white matter; RG, radial glia; VC, ventricular cell.

https://doi.org/10.1371/journal.pbio.2005513.g006

progenies of individual progenitors (S7 Fig; see Methods). Analysis performed at P30 revealed that the tagged cells were GFAP$^+$ astrocytes and included both BG and GLAs, which expressed cell type–specific markers (S8 Fig and S1 Table). Cells were then grouped in clones (see Methods) that resulted to be formed by only BG or both BG and GLAs (Fig 7B, 7C, 7F and 7F'). Clones formed by GLAs only (Fig 7D) were rarely observed and may derive from direct transformation of PCLps into GLAs. The fractions of double BG+GLA clones and BG-only clones were similar, indicating an overall comparable probability for a PCLp to proceed along the 2 lineages (Fig 7E). Double clones were significantly bigger than clones solely formed by BG or GLA (Fig 7G), consistent with the bigger size of StarTrack HetCs. Moreover, double clone average size (about 4.5 cells/clone) and spatial dispersion (about 90% within approximately 180 μm, intraclone intercell distance) were about half of those computed for cortical StarTrack subclones (see above section 'HetCs are formed by a modular architecture'), consistent with tagging of individual progenitors. Notably, the BG:GLA ratio (Fig 7H) revealed a predominance of BG and displayed a value (1.2) intermediate to that of StarTrack triple and double clones.

Similar to VZ RG in the developing telencephalon, the choice of PCLps to self-renew and generate BG or produce a distinct progeny (i.e., GLAs) may be associated with different cleavage plane orientations during division, determining the inheritance of the radial process [21–23]. However, like basal RG [24], phosphorylated Vimentin (pVimentin)-labeled proliferative PCLps always displayed predominant horizontal divisions (S9 Fig) with a frequency (approximately 80%) not matching the proportions of double/BG clones. Thus, factors other than the cleavage plane orientation are likely to influence the PCLp cell fate. In summary, postnatal PCLps can generate GLAs and contribute BG+GLA clones.

Astroglial precursors amplify and differentiate according to layer-specific dynamics after birth

The different sizes of cortical and WMA HomCs and the distinct contribution of astrocyte types to HetCs suggested different layer-specific proliferation rates. This hypothesis was addressed at early postnatal stages, during clone expansion and maximal cerebellar growth [25,26]. Proliferating astroglial progenitors were tagged with 5-ethynyl-2′-deoxyuridine (EdU) in hGFAP-GFP mice [27] (Fig 8A–8D"). EdU$^+$hGFAP$^+$ precursors exhibited layer-dependent proliferative behaviors in both vermis and hemispheres. PCLps divided extensively, showing a peak of proliferation at P1, which gradually decreased afterward. EdU$^+$hGFAP$^+$ cells in the PWM and granular layer (GL) followed the same trend, although with an overall lower proliferation rate (Fig 8A–8D"). A layer-dependent proliferation rate, declining over time, was confirmed when ongoing proliferation was assessed in StarTrack$^+$ cells (S10 Fig). This analysis also indicated a slightly higher proliferative activity in E12-derived PCLps compared to E14 counterparts immediately after birth (S10 Fig). Cell cycle reentry analysis on the whole astrocyte pool (S11A–S11D"' Fig) showed that all astroglial precursors undergo an early

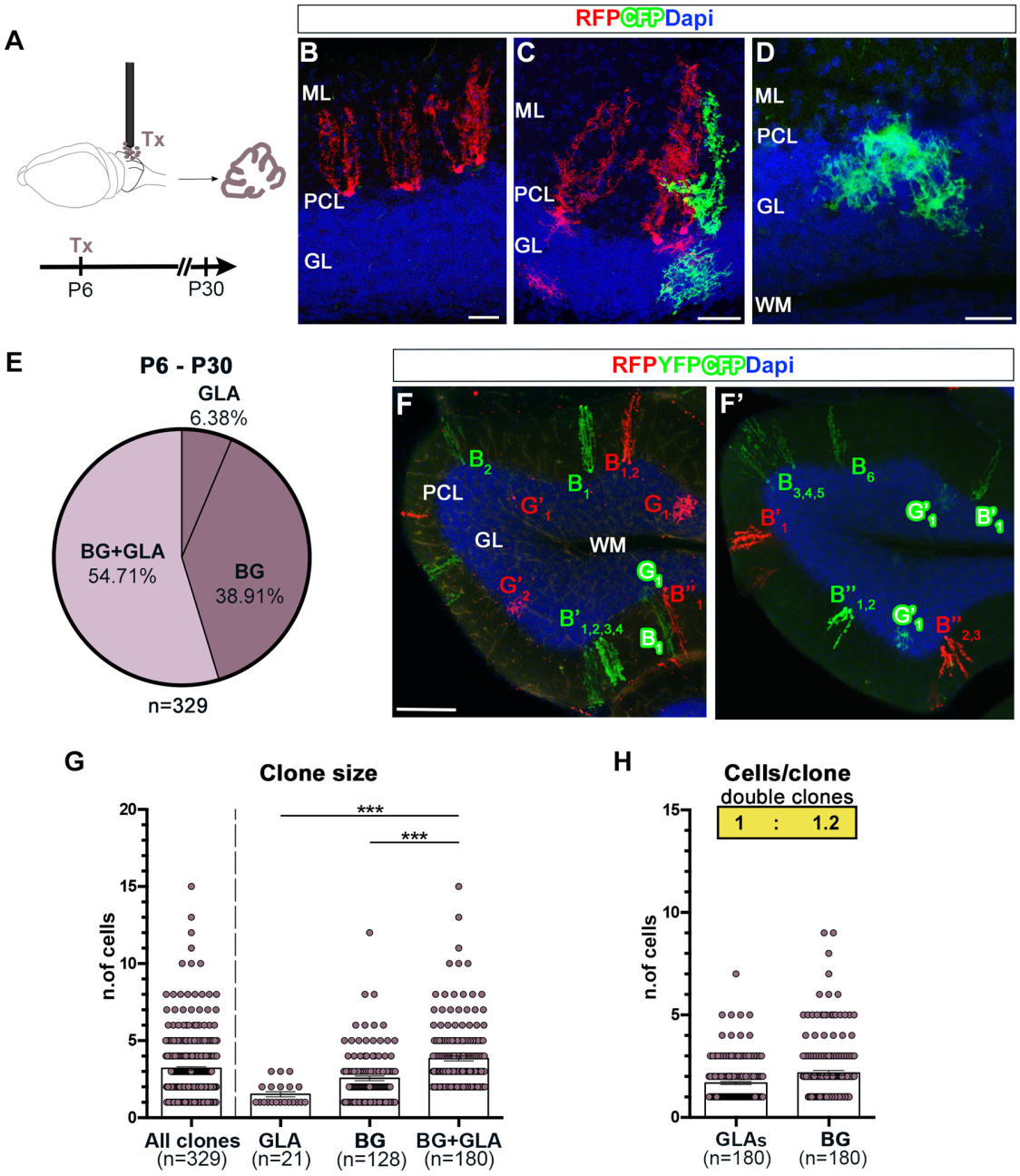

Fig 7. Analysis of PCLp progenies at P30. (A) Experimental design of superficial administration of Tx to induce R26R^{Confetti} recombination in radial GLAST^{+} precursors in the PCL (PCLps). (B-D) Analysis after serial sections' reconstruction at P30 reveals the existence of sister astrocytes (i.e., expressing the same color) arranged in different clone types: BG clones (B), double clones composed of BG+GLA (C), and rare GLA clones (D). (E) Quantification of the relative proportion of each clone type derived from P6-tagged PCLps in lobule IV–V. Pies illustrate pooled data from 3 animals. (F,F') Examples of clones distributed in 1 or 2 adjacent sections. (B = BG, G = GLA; superscripts indicate distinct clones; subscripts indicate sister cells). (G) Scatterplots of clone size. BG+GLA clones are bigger compared to clones composed of only BG or GLAs. (H) Scatterplots show the number of distinct astrocyte types in double clones. The insets report the clonewise stoichiometry, rounded to the first decimal, which highlights the prevalence of BG over GLA. ***, $P < 0.001$; P values are calculated with GEE analysis n = number of clones. Scale bars: 30 μm (B-D), 100 μm (F-F'). The numerical data used in panels (G,H) are included in S1 Data. BG, Bergmann glia; CFP, cyan fluorescent protein; DAPI, 4′,6-diamidino-2-phenylindole; GEE, generalized estimating equations; GL, granular layer; GLA, granular layer astrocyte; GLAST, glutamate aspartate transporter; ML, molecular layer; PCL, Purkinje cell layer; PCLp, Purkinje cell layer precursor; RFP, red fluorescent protein; Tx, tamoxifen; WM, white matter; YFP, yellow fluorescent protein.

https://doi.org/10.1371/journal.pbio.2005513.g007

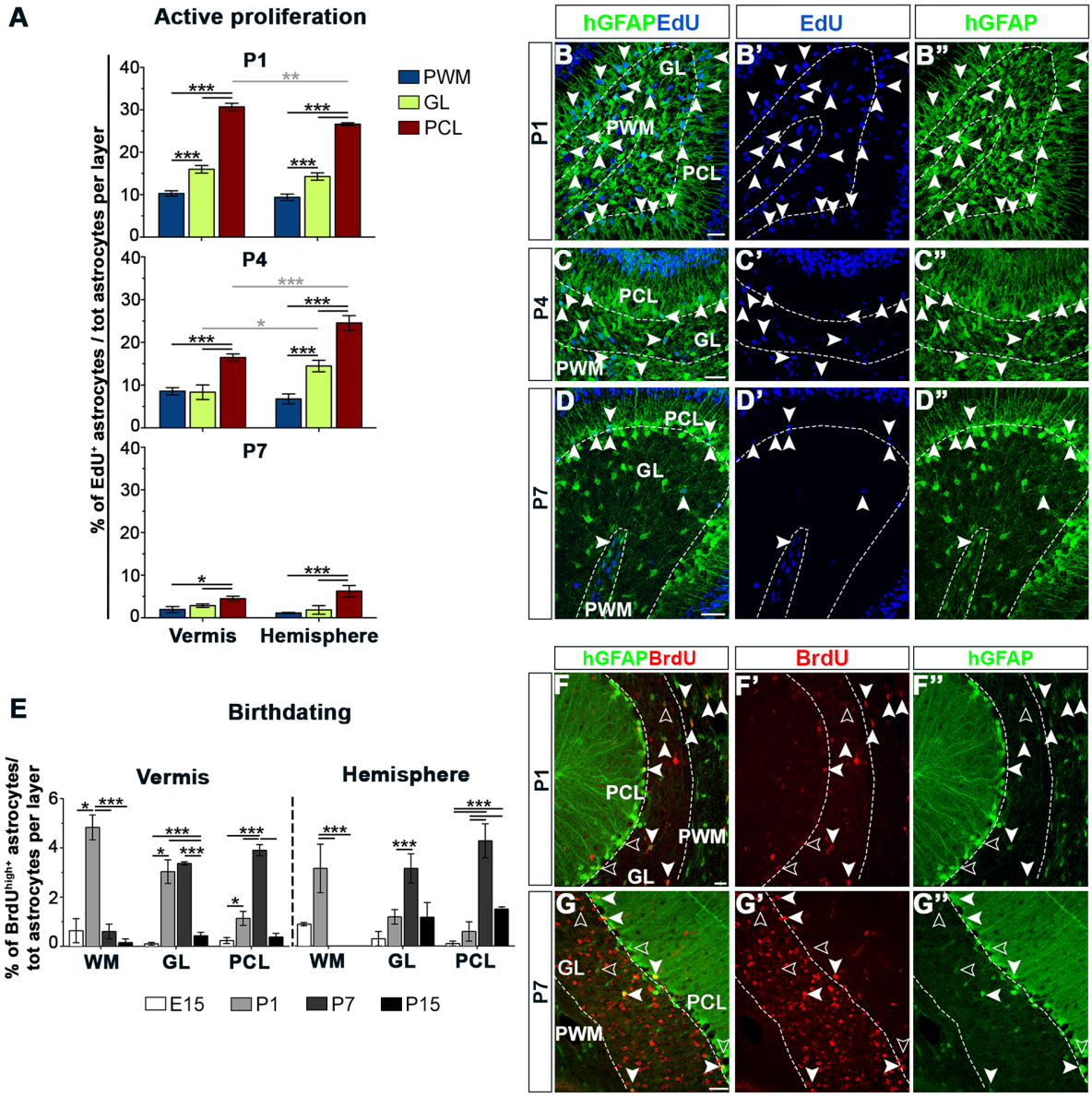

Fig 8. Proliferation and cell cycle exit of cerebellar astrocytes. (A-D) Analysis of active proliferation of astrocytes in different layers during early postnatal development. (A) Percentage of EdU-incorporating astrocyte precursors among total hGFAP$^+$ cells subdivided per layers. EdU was administered 6 h before killing at P1, P4, or P7 to detect actively proliferating cells. At all analyzed time points, proliferation varies among layers and declines over time in both vermis and hemispheres. In B-D", arrowheads point to double-labeled proliferating precursors, highlighting the overall reduction over time in the proliferation activity and the higher number of proliferating cells in the PCL compared to the other layers. (E-G") Birthdating of astrocytes retaining a strong BrdU signal (BrdU^{high}) after the completion of the maturation process (P30). The histogram in (E) shows that the highest percentages of BrdU^{high+} cells are observed in the first postnatal week, with minimal labeling before and afterwards. In detail, numerous WMAs exit the cell cycle already at P1, while GLAs and BG differentiate later. On the whole, this layer-specific pattern applies to both the vermis and the hemispheres ($P = 0.139$), where, however, differentiation delayed (PCL, $P < 0.001$). (F-F", G-G") Full and empty arrowheads point to astrocytes retaining a strong (BrdU^{high}) or a diluted (BrdU^{low}) BrdU signal, respectively. *, $P < 0.05$; **, $P < 0.01$; ***, $P < 0.001$; P values are calculated with GEE analysis. Plots represent data averaged from distinct animals. Scale bars: 30 μm. The numerical data used in panels (A,E) are included in S1 Data. BG, Bergmann glia; BrdU, bromodeoxyuridine; EdU, 5-ethynyl-2′-deoxyuridine; GEE, generalized estimated equations; GL, granular layer; GLA, granular layer astrocyte; hGFAP, human glial fibrillary acidic protein; P, postnatal day; PCL, Purkinje cell layer; PWM, prospective white matter; WM, white matter; WMA, white matter astrocyte.

https://doi.org/10.1371/journal.pbio.2005513.g008

proliferation burst until P4, with PCLps being the most proliferative cells even at later times, consistent with the high number of BG in P30 StarTrack clones. Thus, astroglial progenitors in the postnatal cerebellum undergo intense proliferation immediately after birth and expand according to layer-specific dynamics.

To complement these findings, we performed a birthdating analysis. Retention of high bromodeoxyuridine (BrdU) levels ($BrdU^{high}$) in astrocytes at P30 after a single BrdU pulse identified cells that left the cell cycle approximately at the time of BrdU injection [28]. A remarkably similar layer-dependent differentiation pattern was observed in both vermis and hemispheres. When dividing astrocyte precursors were tagged at E15, rare $BrdU^{high+}hGFAP^{+}$ cells were found at P30, mainly in the WM (Fig 8E and S11E Fig), indicating that E15 progenitors hardly differentiate without further amplification. WMAs predominantly differentiated at P1 (Fig 8E-F"), whereas the bulk of BG and hemispheric GLAs differentiated at the end of the first postnatal week (Fig 8E). Vermian GLAs instead exited proliferation with a constant rate throughout the first 7 d of life (Fig 8E–8G"). $BrdU^{high}$ cells were also found in hemispheric cortical layers when progenitors were tagged at P15, indicating a delay of astrocyte differentiation in this territory. Thus, shortly after birth, WMAs exit the cell cycle, showing a limited expansion phase. Conversely, GLAps continue to divide for a longer time. In addition, PCLps differentiate after an extended expansion during which they appear overall more proliferative compared to progenitors in other layers.

Multipotent and lineage-restricted progenitors are likely to coexist in the E12 and E14 cerebellar VZ

Data show that the cerebellar VZ hosts gliogenic RG producing distinct clone types and whose differentiation potential changes with time and space. These findings could be explained by either distinct RG committed to different fates or by a homogeneous population of multipotent RG that stochastically make their fate choice. To tackle this issue, we tested the validity of a simple model assuming the existence of a single MP pool. To this aim, lineages were simulated in silico, cell fate choices were modeled in a probabilistic manner (Methods; Fig 9A), and the outcome was compared to empirical data. MPs, including both RG and all the precursors in the derived progenies, were assumed to maintain the same properties across layers and over time, whereas the probabilities of production of the distinct astrocyte subtypes were generation-dependently based on birthdating analyses (Fig 9B and S12A Fig).

This stochastic model produced clones whose size was in good agreement with the observed clones (Fig 9C and S12B Fig). However, it failed to reproduce the proportions of clone subtypes and astrocyte types. Indeed, in E12-P30 hemispheric lineages, none of the clone subtypes was correctly captured by the model, except for WMA HomCs, and too many WMAs and BG were produced (Fig 9D–9E). On the other hand, the simulations of E14-P30 vermian families properly reproduced the fraction of the sole double clones but failed with the others and produced too many BG (S12C–S12D Fig). The comparison between the simulated lineages at the generation corresponding to P0 and empirical E12-P0 or E14-P0 clones revealed that at this stage, the amount of simulated HetCs was much higher than expected, while HomCs were underrepresented. The model produced too many PWM+cortical HetCs at P0, at the expense of both cortical and PWM clones (Fig 9F and 9G and S12E–S12F Fig), suggesting a deviation from a model with a single MP already before birth. Overall, these results suggest that the single-MP hypothesis can be ruled out under the assumptions of simple proliferative kinetics and, rather, point towards some additional lineage-restricted progenitor types in the cerebellar VZ.

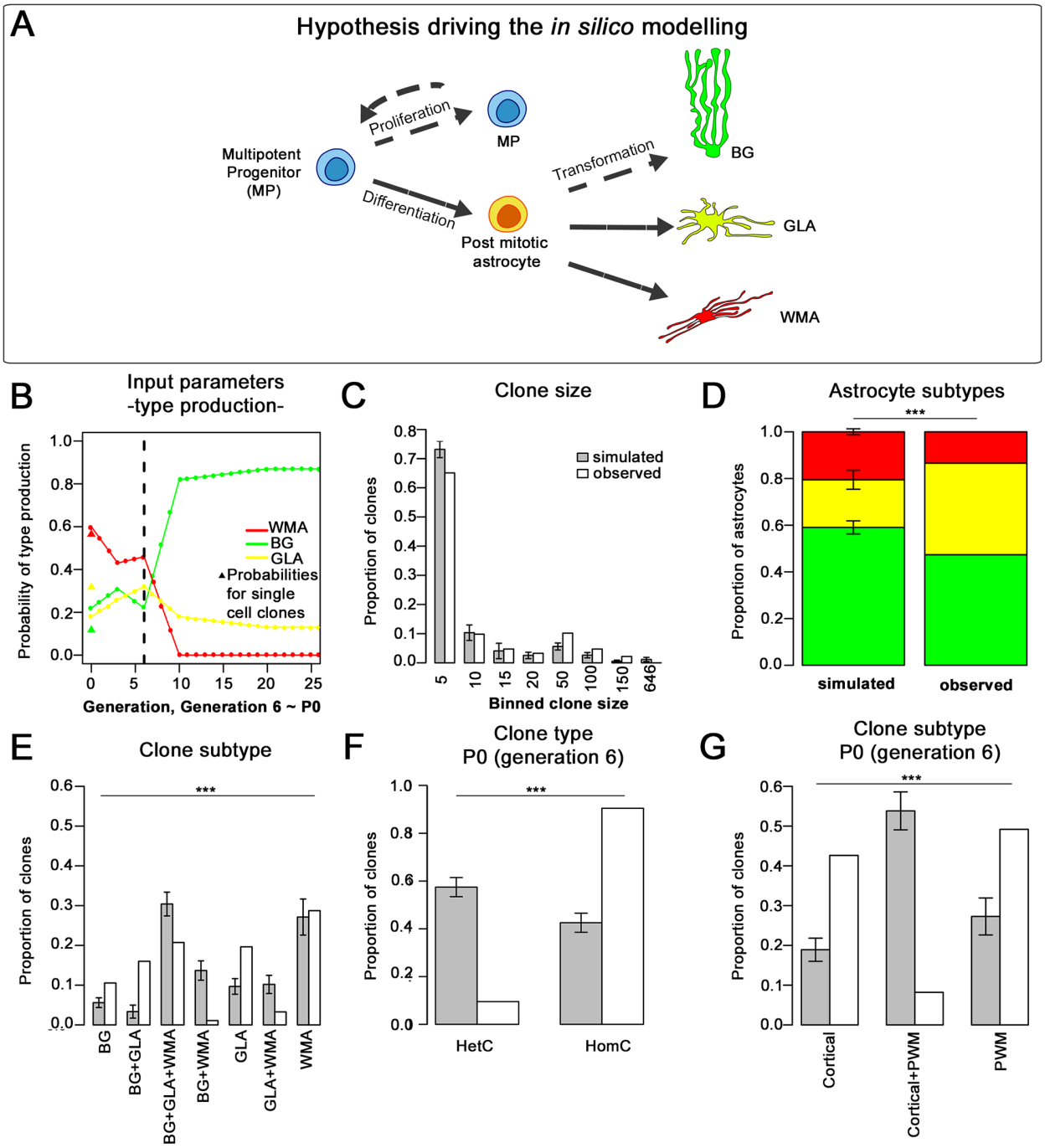

Fig 9. Rules and outcome of the simulation model applied to E12 lineages. (A,B) The schematic representation in (A) shows the distinct fate transitions allowed in the model (indicated by the arrows). The probability of MP proliferation is kept constant at 0.465 in the simulations of E12-P30 lineages. Each daughter cell of each division either remains an MP or differentiates into a postmitotic astrocyte. In this latter case, the probabilities of generating the distinct astrocyte subtypes (BG versus GLA versus WMA) are generation-dependently set according to the birthdating experiments performed in the hemispheres, as shown in (B). Histograms in (C-E) show the outcomes of the simulated lineages compared to the experimental data. Simulated clone sizes (C) appear quite similar to those of the observed clones. On the other hand, the proportions of astrocyte subtypes are not well represented, with too many WMAs and BG produced (D). Same color code as in (A). Similarly, the model fails to recapitulate the proportions of clone subtypes (E; E12-P30). (F,G) Simulated and observed lineages were compared at P0 (corresponding to generation 6). Too many HetCs (F) are found in simulated lineages compared to empirical clones, because of the generation of too many PWM+cortical clones at the expense of both cortical and PWM families (G). ***, $P < 0.001$; P values are calculated with chi-squared test. Cortical clones comprise PCLp HomCs, GLAp HomCs, and PCLp+GLAp

HetCs; Cortical+PWM clones comprise PCLp+PWM, GLAp+PWM, and PCLp+GLAp+PWM HetCs. The numerical data used in panels (B-G) are included in S1 Data. BG, Bergmann glia; E, embryonic day; GLA, granular layer astrocyte; GLAp, granular layer astrocyte precursor; HetC, heterogeneous clone; HomC, homogeneous clone; MP, multiple progenitor; P, postnatal day; PCLp, Purkinje cell layer precursor; PWM, prospective white matter; WMA, white matter astrocyte.

https://doi.org/10.1371/journal.pbio.2005513.g009

Discussion

The spatiotemporal generation pattern of distinct astrocyte types and the rules governing the formation of astroglial lineages are poorly understood. By studying the cerebellum, we found that astrogliogenesis occurs through distinct lineages comprising multiple or single astrocyte types according to an orderly developmental program based on a prominent recurrent modularity in the heterogeneous lineages.

In the mature cerebellum, E12- and E14-derived clones were distributed along the M-L and A-P axes according to a well-defined pattern established at birth and linked to the organization of the cerebellar territory. Clones from E12-tagged RG were found predominantly in the cerebellar hemispheres through all folia, whereas E14-derived RG gave rise to vermian clones, mostly confined to the anterior and posterior lobules. The consistency of this pattern across samples and the rather diffuse M-L and A-P targeting of the VZ by IUE exclude a sample bias. These results are compatible with a developmental scheme where E12 astrogliogenic RG preferentially populate the hemispheres, while distinct RG, still rare at E12, become dominant at later stages, likely by amplification, and populate the vermis. Thus, consecutive waves of RG amplification and detachment seem to occur. This scheme is reminiscent of the organization of cerebellar PCs born on different days and is in line with previous histological findings [11]. Indeed, birthdating studies in rats [14] and genetic fate mapping in mice [16] showed that PC production starts with neurons that, similar to early astrocyte lineages, settle in the hemispheres and paravermis. Along the A-P axis, E14-derived clones were rarely found in the vermian central folia, which might become populated by a distinct wave of astrogliogenesis not sampled in this analysis.

Size and M-L dispersion of individual clones jointly decreased transiting from early hemispheric to later vermian astrogliogenesis and with clone homogeneity. At birth, all clones were small and had similar dispersions and cell type composition, showing that differences predominantly emerge postnatally during cerebellar growth, likely driven by proliferation of pioneer progenitors settled in the nascent parenchyma, as also shown in the forebrain [29]. We also noted that clones were commonly found in a single lobule, in agreement with proliferation occurring within the boundaries of early established fissures anchoring centers, as formerly described for granule cells [25]. E12 triple HetCs were the only exception, showing dispersion across adjacent lobules in the hemispheres. This may depend on delayed hemispheric fissure formation [30] and/or on the presence of numerous PWM multipotent pioneer progenitors. E12 clones were also overall bigger in size compared to E14 families. This, on the one hand, is consistent with the higher proportion of small HomCs in the E14 progeny. On the other hand, E12 progenitors might also be endowed with an increased proliferative capability, which declines in a time-dependent manner in later-generated families, as shown for neurogenic progenitors [31]. Indeed, on the whole, our data suggest that in the hemispheres, a slightly higher proliferative activity in PCLps at defined postnatal time points, together with protracted proliferation leading to a delayed exit from the cell cycle, might contribute to the distinct features of early and late clones. These different behaviors may depend on cell-intrinsic properties or region-specific environmental factors influencing clone proliferation. In this respect, tissue expansion does not appear as the major regulator of clone size, because the vermis, where clones are small, has a volume double of that of each hemisphere. Alternatively, small vermian

clones may just reflect a higher number of RG available to support the full territorial occupation of the vermis. Similarly, the major dispersion of E12 clones may be supported by a specific migratory ability of these early-born progenitors and/or by specific environmental cues, as described to occur in the cerebral cortex [32]. Moreover, radial migration along RG trajectories allocates astrocytes to defined segmental domains according to a temporal ventral-to-dorsal sequence in both the spinal cord and forebrain [1,33]. In the cerebellum, instead, astrocyte allocation over time follows a latero-medial shift that intersects with the formation of the A-P lobular units. Notably, temporal patterning also appears to influence features (e.g., size, dispersion, see also below) of cerebellar astrocyte clones. However, it remains to be determined whether astrocyte spatial segmentation confers a specific functional specialization to the cells.

A characteristic feature of clones was their diverse cell type composition, including homogeneous and heterogeneous lineages constituted of all, 2, or just 1 astroglial type. This highlights a remarkable multipotency of gliogenic RG, which is expressed in terms of both lineages and astroglial types at the examined time points. However, multipotency declines during cerebellar morphogenesis, since triple HetCs became less frequent concomitantly with an expansion of WMA HomCs. The latter finding, as discussed above for size, highlights region-specific differences within the cerebellum. However, it also conforms to the notion of time-dependent reduction in the differentiation potential of neurogenic RG [34,35]. Further, it is suggestive of a progressive separation of cortical and WM lineages, in line with the segregation of astroglial clones found in the neocortex [4]. However, unlike the neocortex, where both cortical and WM clones essentially exhibit a homogeneous composition [4], HetCs consistently comprised the majority of cerebellar astrocytes. The poor morphological diversity of neocortical parenchymal astrocytes may have partly masked clone heterogeneity, which was instead observed in olfactory bulb astroglial clones [36]. These discrepancies may alternatively reflect area-specific differences in RG competence or the occurrence of multipotent gliogenic RG only at early stages of embryonic development. In the cerebellum, HomCs included numerous single-cell clones, consistent with direct derivation of astrocytes from RG without proliferation. This was so far postulated for BG generation through RG translocation [11,12,14], but our data suggest that direct transformation may occur for all astrocyte types and may be especially frequent for WMAs. Some astroglial cerebellar lineages may also contain neuronal derivatives hidden in our data by astrocyte-specific promoter regulation of reporter expression. Based on evidence that postnatal PWM progenitors generate both M-L interneurons and WMAs [15,37,38], sibling interneurons may belong to WMA-containing triple and/or HomCs, although broader clonal relationships between astroglia and other cerebellar neurons cannot be excluded [39].

What mechanisms drive RG along distinct homogeneous or heterogeneous astroglial lineages? The observed behaviors could be produced by a homogeneous population of multipotent RG that undergo stochastic changes in competence over time. Such a model has been proposed [34,35] and confirmed by computational analyses [40,41] for temporal switches in RG fate potency along neuronal lineages. Alternatively, as also suggested for neuronal lineages [42,43] and supported by in silico simulations [31], clone heterogeneity may originate from discrete subsets of RG predetermined toward specific fates, whose relative proportions change with time. The employment of a simple stochastic model suggests that the single-MP hypothesis is not compatible with the observed clonal outcomes under our assumptions. In particular, although a single MP with simple proliferation dynamics is a valid model to explain empirical clone size distribution, it fails to recapitulate the frequencies of nearly all clone subtypes in the simulations of both E12- and E14-P30 lineages, producing overall too many WMAs and/or BG. These results suggest that committed progenitors are also present, enabling a tighter regulation of BG and WMA production. For instance, WMA-related dissimilarities might reflect

the specific properties of bipotent progenitors that produce both WMAs and interneurons [15]. Discrepancies between simulated and empirical lineages could also depend on layer-specific factors biasing cell fate, such as, for instance, the bipotency of PCLps. Moreover, proliferation dynamics may be more complex than the implemented simple proliferative kinetics. Further investigations will allow to clarify these points.

Despite the prominent diversity of clone types, lineages revealed remarkably consistent architectures. First, HomCs were always smaller in size, suggesting a selective divergence of these lineages from HetCs. Second, HetCs showed an analogous stoichiometry in both E12 and E14 families, with few WMAs and similar higher amounts of both BG and GLAs in triple clones and with BG outnumbering GLAs in double clones. Third, and most interestingly, this general architecture was also reflected within individual HetCs, as revealed in E12-P30 clones, where sister cells were mostly organized in subclones. While WMAs appeared to be less prone to cluster with other astrocyte types, the vast majority of these subclones comprised both BG and GLAs and, in turn, displayed a uniform composition, with BG outnumbering GLAs. Thus, subclones with a recurrent relative number of cortical astrocytes may represent a major unitary module upon which HetCs clones are built. The analogous stoichiometry of E12 and E14 clones and similar layer-specific dynamics of vermian and hemispheric astrogliogenesis, as well as PCLp bipotency in both hemisphere and vermis, strongly suggest that the subclone structures found in E12 clones also apply to E14 HetCs. The presence of subclones also prompts the speculation that they may act as functional units, specifically participating in the regulation of defined microcircuits through synchronous calcium fluctuations, similar to functioning of neighboring astrocytes in both the mouse hippocampus and cerebral cortex [44]. Overall, these results indicate that the behavior of gliogenic progenitors in the cerebellum conforms to a remarkably orderly and coordinated program.

How is this stereotyped architecture achieved? Here we identify 2 contributing factors: (i) Distinct layer-dependent rhythms of astrocyte amplification and cell cycle exit, which well fit the clone/subclone architectures. Namely, WMAs leave the cell cycle early while proliferation in cortical layers is more intense and lasts longer, especially in the PCL, in parallel with the tangential expansion of the cerebellar surface. Distinct molecular machineries could sustain different rhythms, as suggested by evidence that PCL and PWM astroglial progenitors rely on different types of cyclins D [15]. Yet, cell-extrinsic factors are likely to modulate these behaviors. Neuron-derived signals are known to affect cerebellar astrocyte proliferation, differentiation, and acquisition of layer-specific phenotypic traits [7,45–47], thereby possibly taking part also in layer-specific dynamics. In particular, Sonic hedgehog (SHH) derived from PCs is able to induce the neurochemical conversion of GLAs into BG [7]. Shh is thus an obvious candidate for a cortical layer–specific cue that can bias the differentiation propensity of PCLps toward BG over GLAs. (ii) PCLps are not exclusively committed to the BG fate and can give rise to clones containing both BG and GLAs. Thus, PCLps appear as the most likely source of double HetCs and BG+GLA containing subclones, but this hypothesis remains to be directly demonstrated. This interpretation is in agreement with findings in mutants where bona fide BG progenitors (here named PCLps) fail to develop, with consequent prominent loss not only of BG but also of GLAs [13,48]. Moreover, the gliogenic plasticity of PCLps fits well the adaptive reprogramming shown for these progenitors after a major depletion of the perinatal external granular cell layer (EGL) [49]. Further, PCLp horizontal cleavage plane orientations establish a similarity to neocortical basal RG [24,50–52], which adds to former evidence of phenotypic [53] and functional (i.e., contribution to folding [13,48,54]) relationships between these 2 basally anchored progenitors. In sum, our results point to PCLp as the fundamental organizing element of cortical components in HetCs. In addition, we speculate that part of these basal progenitors after detachment from the VZ and before reaching the PCL could divide and also

individual clones among BG HomCs are less frequent (Fisher's exact test shows a statistically significant difference between WM and BG in E12-P30 clones; *, $P = 0.0265$). n = number of clones. The numerical data used in panels (A,B,E,F) are included in S1 Data. BG, Bergmann glia; HomC, homogeneous clone; E, embryonic day; GLA, granular layer astrocyte; IUE, in utero electroporation; WM, white matter; WMA, white matter astrocyte.
(TIF)

S6 Fig. Expression of lineage markers in StarTrack-labeled cells at P0. (A,B) At P0, StarTrack-labeled astrocytes found in both the cerebellar cortex (A) and PWM (B) express the astrocyte progenitor marker BLBP [8] (the white color in A' and B' indicates the colocalization at the pixel level between StarTrack GFP and BLBP). (C,C') In the PWM, electroporated cells also express NFIA [19], further confirming their identity as astrocyte progenitors. (D,E) In parallel, absence of PAX2 (D,D') and SOX10 (E,E') staining in StarTrack-labeled progenitors exclude that they belong to the interneuron or oligodendroglial lineage, respectively [15,18]. Scale bars: 30 μm. BLBP, brain lipid–binding protein; GFP, green fluorescent protein; GL, granular layer; NFIA, nuclear factor 1 A; P, postnatal day; PAX2, paired box gene 2; PCL, Purkinje cell layer; PWM, prospective white matter; SOX10, SRY-box 10.
(TIF)

S7 Fig. Short-term analysis of Confetti-labeled cells and comparisons with P30 data. (A) Low magnification of lobule IV–V 48 h after local administration of Tx at P6. Arrows point to sparse PCLps labeled with different Confetti colors (RFP, red arrowheads; YFP, green-filled arrowheads; CFP, white arrowhead with green contour). The position of the cell body in the PCL, the radial morphology and the expression of the astroglial marker BLBP (B-C') confirm that cells tagged by Tx are PCLps. As expected, PCLps are negative for the oligodendroglial marker SOX10 (D, D'). (E-G') At short term, the vast majority of the cells (about 80%) are single PCLp, but some pairs of sister cells are also visible. They are composed of 2 juxtaposed cells of the same color. In some cases, they are about to complete a mitosis (nuclei in late telophase in E and relative inset), or splitting apart (F,F'). In other cases, both cells are still in the cell cycle; as assessed by Ki67 expression, they display similar configuration of the nuclei and a mirror morphology, elements indicative of cell division (G, G' and relative insets). Yellow dotted lines in the insets in E, F, G highlight $Ki67^+$ nuclei of duplets. One of the 2 cells in pairs always displays a PCLp feature, while the other one, in some cases, seems to extend stellate-like processes, suggestive of a GLA fate (arrowheads in F' and G'). The histogram in H represents the distribution of the mean extensions of clones identified at P30 (single-cell clones were excluded; bin size = 15 μm). The estimated minimal distance between clones (317 μm, red dotted line) is significantly higher than the mean clone extension (104 μm, black dotted line; $P < 0.001$), and only a small fraction of clones have an extension close to the minimal inter-clone distance (see Methods). Scale bars 20 μm and 100 μm in A. The numerical data used in panel (H) are included in S1 Data. BLBP, brain lipid–binding protein; CFP, cyan fluorescent protein; GL, granular layer; P, postnatal day; PCL, Purkinje cell layer; PCLp, Purkinje cell layer precursor; RFP, red fluorescent protein; SOX10, SRY-box 10; Tx, tamoxifen; YFP, yellow fluorescent protein.
(TIF)

S8 Fig. Expression of lineage and astrocyte type–specific markers in P30 Confetti-labeled cells. (A,B) Cells labeled after in situ Tx administration in Confetti mice are $GFAP^+$ astrocytes in the PCL (A1 and B1,2) or in the GL (A2). (C-F) The morphological and spatial criteria used to identify BG or GLA are validated by the expression of astrocyte type–specific markers [7,76] (see S1 Table). BG (C-C'), but not GLAs (D-D'), express high levels of GLAST and are also

positive for the BG-specific marker GDF10 (E-E'). Asterisks in C' highlight the cell body of GLAST-negative Purkinje cells surrounded by GLAST-positive BG processes. (F-F") On the contrary, AQP4 stains exclusively astrocytes in the GL (F2,3) but not BG (F1). Both BG (G-G') and GLAs (H-H') do not express the oligodendrocyte marker Sox10, confirming their astrocytic identity. A'-A", B'-B", C'-D',E',F', F" are single-step confocal images that more clearly demonstrate the specificity of the different stainings in Confetti-positive or negative (G'-H') cells. Arrowheads point to Confetti$^+$ cells. Scale bars: 20 μm. AQP4, aquaporin 4; BG, Bergmann cell; GDF10, growth differentiation factor 10; GL, granular layer; GLA, granular layer astrocyte; GLAST, glutamate aspartate transporter; P, postnatal day; PCL, Purkinje cell layer; SOX10, SRY-box 10; Tx, tamoxifen; WM, white matter.
(TIF)

S9 Fig. Cleavage plane orientation of PCLps. (A) Frequency distribution of the cleavage plane orientations in pVimentin$^+$ PCLp at different time points. PCLps preferentially divide with a cleavage plane horizontal to the PCL throughout cerebellar development (***, $P < 0.001$). No statistically significant differences are found in the distribution of cleavage plane orientations over time ($P = 0.107$, main effect of time). (B) During late embryonic phases, radial progenitors delaminate from the VZ and start to colonize the developing PCL and keep dividing through horizontal divisions. (C-D') After birth, proliferating PCLps still maintain a horizontal cleavage plane, independently of the position of the radial process (highlighted by yellow arrowheads). (D') Magnification of a single confocal plane of the pVimentin$^+$ cell in D to show the cleavage plane orientation of the nucleus during telophase. *P* values are computed with GEE analysis. Scale bars: 20 μm (B-D), 10 μm (D'). The numerical data used in panel (A) are included in S1 Data. EGL, external granular layer; GEE, generalized estimated equations; PCL, Purkinje cell layer; PCLp, Purkinje cell layer precursor; pVimentin, phosphorylated Vimentin; VZ, ventricular zone.
(TIF)

S10 Fig. Active proliferation of StarTrack-labeled astrocyte progenitors. Analysis of active proliferation was performed on E12 hemispheric (green) or E14 vermian (orange) StarTrack-tagged cells in different layers during early postnatal development. Mice were administered twice with EdU with a 3-h interval, and the percentage of EdU-incorporating astrocyte precursors over the total amount of StarTrack-labeled cells in each layer was calculated. At both P1 (A) and P4 (B), the tagged progenitors show a layer-specific pattern of proliferation that declines over time. E12-tagged (green) astrocyte progenitors in the PCL show a slightly higher proliferation activity at P1 (A) compared to those electroporated at E14 (orange). On the other hand, at P4 (B), E12-tagged progenitors in the PWM and GL show a trend to be more proliferative compared to their E14-tagged counterparts, although the low number of cells does not allow to reveal a statistical significance. *, $P < 0.05$; **, $P < 0.01$; ***, $P < 0.001$; *P* values are calculated with Fisher's exact test. *n* = number cells. The numerical data used in the figure are included in S1 Data. E, embryonic day; EdU, 5-ethynyl-2′-deoxyuridine; GL, granular layer; P, postnatal day; PCL, Purkinje cell layer; PWM, prospective white matter.
(TIF)

S11 Fig. Proliferation dynamics of postnatal astroglial progenitors. (A) Experimental design: BrdU was injected at P1 or P4 in hGFAP-GFP mice and EdU 6 h before killing at P4 or P7. Triple-labeled cells analyzed in the vermis were plotted as the percentage of total BrdU$^+$/hGFAP$^+$ cells per layer. At each time point, PCLps reenter more frequently in the cell cycle compared to astrocyte precursors in other layers. In the PWM from P4 on, there is a significant drop in the proportion of astrocytes performing another division. The same trend is also

present, though less evident, in the GL. (B-D"') Images represent sagittal sections of cerebella at the different time points analyzed after double thymidine analogue labeling: (B-B"') P1–P4, (C-C"') P4–P7, and (D-D"') P1–P7. Merged and single channels for BrdU (red), EdU (blue), and GFP (hGFAP, green) stainings are presented. Arrowheads point to some triple-labeled cells. (E-G) Representative images of P30 cerebella of mice injected with BrdU at the beginning (E15, E) and the end (P15, F,G) of astroglial development. Full and empty arrowheads indicate cells with $BrdU^{high}$ or $BrdU^{low}$ positivity, respectively. Plots represent data averaged from distinct animals. *, $P < 0.05$; ***, $P < 0.001$, calculated with GEE analysis. Scale bars: 30 μm. The numerical data used in panel (A) are included in S1 Data. BrdU, bromodeoxyuridine; EdU, 5-ethynyl-2′-deoxyuridine; GEE, generalized estimated equations; GFP, green fluorescent protein; GL, granular layer; hGFAP, human glial fibrillary acidic protein; P, postnatal day; PCL, Purkinje cell layer; PCLp, Purkinje cell layer precursor; PWM, prospective white matter; WM, white matter.
(TIF)

S12 Fig. Simulations of E14 lineages. The probabilities for a differentiating progenitor of generating the distinct astrocyte subtypes (BG versus GLA versus WMA) are generation-dependently set according to the birthdating experiments performed in the vermis, as shown in (A). Histograms in (B-D) show the outcomes of the simulated lineages compared to the experimental data. Simulated clone sizes (B) appear quite similar to those of the observed clones. On the other hand, the model fails to recapitulate the proportions of astrocyte subtypes, with the production of too many BG (C; same color code as in A). Similarly, the model fails with the proportions of clone subtypes (D). (E,F) Simulated and observed lineages were compared at P0 (corresponding to generation 4). Too many HetCs (E) are simulated compared to empirical clones, because of the generation of too many PWM+cortical clones at the expenses of either cortical and PWM families (F). ***, $P < 0.001$, P values were calculated with chi-squared test. Cortical clones comprise PCLp HomCs, GLAp HomCs and PCLp +GLAp HetCs; Cortical+PWM clones comprise PCLp+PWM, GLAp+PWM, and PCLp +GLAp+PWM HetCs. The numerical data used in panels (A-F) are included in S1 Data. BG, Bergmann glia; E, embryonic day; GLA, granular layer astrocyte; GLAp, granular layer astrocyte precursor; HetC, heterogeneous clone; HomC, homogeneous clone; P, postnatal day; PCLp, Purkinje cell layer precursor; PWM, prospective white matter; WMA, white matter astrocyte.
(TIF)

S13 Fig. GFAP immunostaining confirms the astrocytic identity of labeled cells. (A,B) Reslices of single step images of P30 clones after anti-GFAP staining (white/purple) unequivocally show the astrocytic identity of cells labeled solely with nuclear markers. Scale bars: 30 μm. GFAP, glial fibrillar acidic protein; P, postnatal day.
(TIF)

S14 Fig. Impact of clones defined by repeated combinations on features of E12 HetCs with the highest lumping errors. The repeated frequency of some combinations suggests that these may be less reliable to define sibling cells in our samples. Therefore, we assessed whether the clones defined by these repeated combinations in the samples found more prone to lumping errors (2 samples of E12 clones that underwent cluster analysis) belonged to specific clone types/subtypes and displayed features introducing a systematic bias in the analyses. (A) Repeated combinations were homogeneously represented among the distinct clone types/subtypes, with the only exception of BG+GLA+WMA+CNA clones, in which they were enriched (chi test, $P = 0.025$). However, this clone type, being very rare, was not included in quantitative

analyses. (B) Clones defined by repeated combinations (blue bars) were not different from the whole populations (black bars) and behaved as clones with unique combinations (red bars) in terms of clone size ($P > 0.05$), which is a key clone feature. These results suggest that the presence in the examined samples of clones labeled by repeated combinations does not significantly affect results. The numerical data used in panel (B) are included in S1 Data. E, embryonic day; HetC, heterogeneous clone.
(TIF)

S15 Fig. Impact of potential clustering errors. Because of the possible presence of a nonnegligible clustering error, we estimated the impact of a subclone identification bias by rerunning the cluster analysis varying by 20% the number of identified subclones (this was empirically achieved by using 90% and 99% accounted variance thresholds). The ensuing changes in subclone type distributions and ratio were negligible (cf. Fig 5E–5H). The numerical data used in the figure are included in S1 Data.
(TIF)

S1 Table. Heterogeneity in major astrocyte types.
(DOCX)

S2 Table. List of StarTrack clones and measured parameters.
(XLSX)

S3 Table. Repeated combinations and probabilities of lumping errors.
(DOCX)

S4 Table. List of Confetti clones, measured parameters, and short-term analysis.
(XLSX)

S5 Table. Statistical analyses.
(XLSX)

S1 Data. Excel spreadsheet containing, in separate sheets, the underlying numerical data of Figs 3A, 3B, 3C, 3D, 4A, 4B, 4C, 4D, 5A, 5E, 5F, 5G, 5H, 6D, 6E, 7G, 7H, 8A, 8E and 9B, 9C, 9D, 9E, 9F, 9G, S3A, S3B, S4A, S4B, S5A, S5B, S5E, S5F, S7H, S9A, S10A, S10B, S11A, S12A S12B, S12C, S12D, S12E, S12F, S14B and S15.
(XLSX)

Acknowledgments

We are grateful to Prof. Paolo Provero for helpful discussion on statistical analyses and to Drs. Enrica Boda, Claudio Giachino, and Chiara Rolando for critically reading the manuscript. We are also deeply indebted to Münevver Aksoy for technical assistance.

Author Contributions

Conceptualization: Valentina Cerrato, Elena Parmigiani, Annalisa Buffo.

Data curation: Valentina Cerrato, Elena Parmigiani, Ishira Nanavaty, Claudio de'Sperati.

Formal analysis: Valentina Cerrato, Elena Parmigiani, Marion Betizeau, Jessica Aprato, Paola Berchialla, Claudio de'Sperati, Annalisa Buffo.

Funding acquisition: Annalisa Buffo.

Investigation: Valentina Cerrato, Elena Parmigiani, María Figueres-Oñate.

Methodology: Valentina Cerrato, Elena Parmigiani, María Figueres-Oñate, Marion Betizeau, Paola Berchialla, Claudio de'Sperati, Laura López-Mascaraque, Annalisa Buffo.

Project administration: Annalisa Buffo.

Supervision: Annalisa Buffo.

Visualization: Valentina Cerrato, Elena Parmigiani, Federico Luzzati.

Writing – original draft: Valentina Cerrato, Elena Parmigiani, Annalisa Buffo.

Writing – review & editing: Valentina Cerrato, Elena Parmigiani, María Figueres-Oñate, Marion Betizeau, Ishira Nanavaty, Claudio de'Sperati, Laura López-Mascaraque, Annalisa Buffo.

References

1. Bayraktar OA, Fuentealba LC, Alvarez-Buylla A, Rowitch DH. Astrocyte development and heterogeneity. Cold Spring Harb Perspect Biol. 2015; 7(1) a020362. https://doi.org/10.1101/cshperspect.a020362 PMID: 25414368
2. Ben Haim L, Rowitch D. Functional diversity of astrocytes in neural circuit regulation. Nat Rev Neurosci. 2016; 18(1):31–41. https://doi.org/10.1038/nrn.2016.159 PMID: 27904142
3. John Lin C-C, Yu K, Hatcher A, Huang T-W, Lee HK, Carlson J, et al. Identification of diverse astrocyte populations and their malignant analogs. Nat Neurosci. 2017; 20(3): 396–405. https://doi.org/10.1038/nn.4493 PMID: 28166219
4. García-Marqués J, López-Mascaraque L. Clonal identity determines astrocyte cortical heterogeneity. Cereb Cortex. 2012; 23(6):1463–72. https://doi.org/10.1093/cercor/bhs134 PMID: 22617854
5. Bribián A, Figueres-Oñate M, Martín-López E, López-Mascaraque L. Decoding astrocyte heterogeneity: New tools for clonal analysis. Neuroscience. 2016; 323(Supplement C):10–9. https://doi.org/10.1016/j.neuroscience.2015.04.036 PMID: 25917835
6. Magavi S, Friedmann D, Banks G, Stolfi A, Lois C. Coincident generation of pyramidal neurons and protoplasmic astrocytes in neocortical columns. J Neurosci. 2012 Apr; 32(14):4762–72. https://doi.org/10.1523/JNEUROSCI.3560-11.2012 PMID: 22492032
7. Farmer WT, Abrahamsson T, Chierzi S, Lui C, Zaelzer C, Jones E V, et al. Neurons diversify astrocytes in the adult brain through sonic hedgehog signaling. Science. 2016 Feb 19; 351(6275):849–54. https://doi.org/10.1126/science.aab3103 PMID: 26912893
8. Buffo A, Rossi F. Origin, lineage and function of cerebellar glia. Prog Neurobiol. 2013 Oct; 109:42–63. https://doi.org/10.1016/j.pneurobio.2013.08.001 PMID: 23981535
9. Palay S, Chan-Palay V. Cerebellar Cortex. New York: Springer-Verlag Berlin Heidelberg; 1974.
10. Ramon y Cajal S. Histologie du Système Nerveux de l'Homme et des Vertébrés. Maloine, Paris; 1911.
11. Yuasa S. Bergmann glial development in the mouse cerebellum as revealed by tenascin expression. Anat Embryol (Berl). 1996; 194(3):223–34. PMID: 8849669
12. Yamada K, Watanabe M. Cytodifferentiation of Bergmann glia and its relationship with Purkinje cells. Anat Sci Int. 2002 Jun; 77(2):94–108. https://doi.org/10.1046/j.0022-7722.2002.00021.x PMID: 12418089
13. Li K, Leung AW, Guo Q, Yang W, Li JYH. Shp2-dependent ERK signaling is essential for induction of Bergmann glia and foliation of the cerebellum. J Neurosci. 2014 Jan 15; 34(3):922–31. https://doi.org/10.1523/JNEUROSCI.3476-13.2014 PMID: 24431450
14. Altman J, Bayer SA. Development of the Cerebellar System in Relation to its Evolution, Structure and Functions. CRC Press, New York, NY, 1997.
15. Parmigiani E, Leto K, Rolando C, Figueres-Oñate M, López-Mascaraque L, Buffo A, et al. Heterogeneity and Bipotency of Astroglial-Like Cerebellar Progenitors along the Interneuron and Glial Lineages. J Neurosci. 2015; 35(19):7388–402. https://doi.org/10.1523/JNEUROSCI.5255-14.2015 PMID: 25972168
16. Sudarov A, Turnbull RK, Kim EJ, Lebel-Potter M, Guillemot F, Joyner AL. Ascl1 genetics reveals insights into cerebellum local circuit assembly. J Neurosci. 2011 Jul 27; 31(30):11055–69. https://doi.org/10.1523/JNEUROSCI.0479-11.2011 PMID: 21795554

17. Kita Y, Kawakami K, Takahashi Y, Murakami F. Development of cerebellar neurons and glias revealed by in utero electroporation: Golgi-like labeling of cerebellar neurons and glias. PLoS ONE. 2013; 8(7): e70091. https://doi.org/10.1371/journal.pone.0070091 PMID: 23894597

18. Hashimoto R, Hori K, Owa T, Miyashita S, Dewa K, Masuyama N, et al. Origins of oligodendrocytes in the cerebellum, whose development is controlled by the transcription factor, Sox9. Mech Dev. 2016 May; 140:25–40. https://doi.org/10.1016/j.mod.2016.02.004 PMID: 26940020

19. Deneen B, Ho R, Lukaszewicz A, Hochstim CJ, Gronostajski RM, Anderson DJ. The transcription factor NFIA controls the onset of gliogenesis in the developing spinal cord. Neuron. 2006 Dec; 52(6):953–68. https://doi.org/10.1016/j.neuron.2006.11.019 PMID: 17178400

20. Snippert HJ, van der Flier LG, Sato T, van Es JH, van den Born M, Kroon-Veenboer C, et al. Intestinal crypt homeostasis results from neutral competition between symmetrically dividing Lgr5 stem cells. Cell. 2010 Oct 1; 143(1):134–44. https://doi.org/10.1016/j.cell.2010.09.016 PMID: 20887898

21. Miyata T, Kawaguchi A, Okano H, Ogawa M. Asymmetric inheritance of radial glial fibers by cortical neurons. Neuron. 2001 Sep; 31(5):727–41. https://doi.org/10.1016/S0896-6273(01)00420-2 PMID: 11567613

22. Gotz M, Huttner WB. The cell biology of neurogenesis. Nat Rev Mol Cell Biol. 2005 Oct; 6(10):777–88. https://doi.org/10.1038/nrm1739 PMID: 16314867

23. Konno D, Shioi G, Shitamukai A, Mori A, Kiyonari H, Miyata T, et al. Neuroepithelial progenitors undergo LGN-dependent planar divisions to maintain self-renewability during mammalian neurogenesis. Nat Cell Biol. 2008 Jan; 10(1):93–101. https://doi.org/10.1038/ncb1673 PMID: 18084280

24. Wang X, Tsai J-W, LaMonica B, Kriegstein AR. A new subtype of progenitor cell in the mouse embryonic neocortex. Nat Neurosci. 2011 May; 14(5):555–61. https://doi.org/10.1038/nn.2807 PMID: 21478886

25. Legué E, Riedel E, Joyner AL. Clonal analysis reveals granule cell behaviors and compartmentalization that determine the folded morphology of the cerebellum. Development. 2015 May 1; 142(9):1661–71. https://doi.org/10.1242/dev.120287 PMID: 25834018

26. de Luca A, Vassallo S, Benitez-Temino B, Menichetti G, Rossi F, Buffo A. Distinct modes of neuritic growth in Purkinje neurons at different developmental stages: Axonal morphogenesis and cellular regulatory mechanisms. PLoS ONE. 2009; 4(8): e6848. https://doi.org/10.1371/journal.pone.0006848 PMID: 19718257

27. Zhuo L, Sun B, Zhang C, Fine A. Live Astrocytes Visualized by Green Fluorescent Protein in Transgenic Mice. Dev Biol. 1997; 42:36–42.

28. Rolando C, Parolisi R, Boda E, Schwab ME, Rossi F, Buffo A. Distinct Roles of Nogo-A and Nogo Receptor 1 in the Homeostatic Regulation of Adult Neural Stem Cell Function and Neuroblast Migration. J Neurosci. 2012; 32(49):17788–99. https://doi.org/10.1523/JNEUROSCI.3142-12.2012 PMID: 23223298

29. Ge W-P, Miyawaki A, Gage FH, Jan YN, Jan LY. Local generation of glia is a major astrocyte source in postnatal cortex. Nature. 2012 Apr 19; 484(7394):376–80. https://doi.org/10.1038/nature10959 PMID: 22456708

30. Cheng Y, Sudarov A, Szulc KU, Sgaier SK, Stephen D, Turnbull DH, et al. The Engrailed homeobox genes determine the different foliation patterns in the vermis and hemispheres of the mammalian cerebellum. Development. 2010 Feb; 137(3):519–29. https://doi.org/10.1242/dev.027045 PMID: 20081196

31. Gao P, Postiglione MP, Krieger TG, Hernandez L, Wang C, Han Z, et al. Deterministic progenitor behavior and unitary production of neurons in the neocortex. Cell. 2014; 159(4):775–88. https://doi.org/10.1016/j.cell.2014.10.027 PMID: 25417155

32. Jacobsen CT, Miller RH. Control of astrocyte migration in the developing cerebral cortex. Dev Neurosci. 2003; 25(2–4):207–16. https://doi.org/10.1159/000072269 PMID: 12966218

33. Tsai H-H, Li H, Fuentealba LC, Molofsky A V, Taveira-Marques R, Zhuang H, et al. Regional astrocyte allocation regulates CNS synaptogenesis and repair. Science. 2012 Jul 20; 337(6092):358–62. https://doi.org/10.1126/science.1222381 PMID: 22745251

34. Shen Q, Wang Y, Dimos JT, Fasano CA, Phoenix TN, Lemischka IR, et al. The timing of cortical neurogenesis is encoded within lineages of individual progenitor cells. Nat Neurosci. 2006 Jun; 9(6):743–51. https://doi.org/10.1038/nn1694 PMID: 16680166

35. Guo C, Eckler MJ, McKenna WL, McKinsey GL, Rubenstein JLR, Chen B. Fezf2 expression identifies a multipotent progenitor for neocortical projection neurons, astrocytes, and oligodendrocytes. Neuron. 2013 Dec; 80(5):1167–74. https://doi.org/10.1016/j.neuron.2013.09.037 PMID: 24314728

36. Garcia-Marques J, Lopez-Mascaraque L. Clonal Mapping of Astrocytes in the Olfactory Bulb and Rostral Migratory Stream. Cereb Cortex. 2017 Mar; 27(3):2195–209. https://doi.org/10.1093/cercor/bhw071 PMID: 27001681

37. Silbereis J, Cheng E, Ganat YM, M LR, and Vaccarino FM. Precursors with GFAP promoter activity transiently generate GABA interneurons in the postnatal cerebellum. Stem Cells. 2009; 27(5):1152–63. https://doi.org/10.1002/stem.18 PMID: 19418461

38. Fleming JT, He W, Hao C, Ketova T, Pan FC, Wright CC V, et al. The Purkinje Neuron Acts as a Central Regulator of Spatially and Functionally Distinct Cerebellar Precursors. Dev Cell. 2013; 27(3):278–92. https://doi.org/10.1016/j.devcel.2013.10.008 PMID: 24229643

39. Lin JC, Cepko CL. Biphasic dispersion of clones containing Purkinje cells and glia in the developing chick cerebellum. Dev Biol. 1999 Jul 15; 211(2):177–97. https://doi.org/10.1006/dbio.1999.9316 PMID: 10395781

40. Gomes FLAF, Zhang G, Carbonell F, Correa JA, Harris WA, Simons BD, et al. Reconstruction of rat retinal progenitor cell lineages in vitro reveals a surprising degree of stochasticity in cell fate decisions. Development. 2011; 138(2):227–35. https://doi.org/10.1242/dev.059683 PMID: 21148186

41. He J, Zhang G, Almeida AD, Cayouette M, Simons BD, Harris WA. How Variable Clones Build an Invariant Retina. Neuron. 2012; 75(5):786–98. https://doi.org/10.1016/j.neuron.2012.06.033 PMID: 22958820

42. Franco SJ, Gil-Sanz C, Martinez-Garay I, Espinosa A, Harkins-Perry SR, Ramos C, et al. Fate-restricted neural progenitors in the mammalian cerebral cortex. Science. 2012 Aug; 337(6095):746–9. https://doi.org/10.1126/science.1223616 PMID: 22879516

43. Ciceri G, Dehorter N, Sols I, Huang ZJ, Maravall M, Marin O. Lineage-specific laminar organization of cortical GABAergic interneurons. Nat Neurosci. 2013 Sep; 16(9):1199–210. https://doi.org/10.1038/nn.3485 PMID: 23933753

44. Sasaki T, Kuga N, Namiki S, Matsuki N, Ikegaya Y. Locally synchronized astrocytes. Cereb Cortex. 2011 Aug; 21(8):1889–900. https://doi.org/10.1093/cercor/bhq256 PMID: 21212170

45. Hatten ME. Neuronal regulation of astroglial morphology and proliferation in vitro. J Cell Biol. 1985 Feb; 100(2):384–96. PMID: 3881455

46. Nagata I, Keilhauer G, Schachner M. Neuronal influence on antigenic marker profile, cell shape and proliferation of cultured astrocytes obtained by microdissection of distinct layers from the early postnatal mouse cerebellum. Brain Res. 1986 Jan; 389(1–2):217–32. PMID: 3484997

47. Eiraku M, Tohgo A, Ono K, Kaneko M, Fujishima K, Hirano T, et al. DNER acts as a neuron-specific Notch ligand during Bergmann glial development. Nat Neurosci. 2005 Jul; 8(7):873–80. https://doi.org/10.1038/nn1492 PMID: 15965470

48. Leung AW, Li JYH. The Molecular Pathway Regulating Bergmann Glia and Folia Generation in the Cerebellum. 2018 Feb; 17(1):42–48. https://doi.org/10.1007/s12311-017-0904-3 PMID: 29218544

49. Wojcinski A, Lawton AK, Bayin NS, Lao Z, Stephen DN, Joyner AL. Cerebellar granule cell replenishment postinjury by adaptive reprogramming of Nestin + progenitors. Nat Neurosci. 2017 Oct; 20(10):1361–1370. https://doi.org/10.1038/nn.4621 PMID: 28805814

50. Betizeau M, Cortay V, Patti D, Pfister S, Gautier E, Bellemin-Menard A, et al. Precursor diversity and complexity of lineage relationships in the outer subventricular zone of the primate. Neuron. 2013 Oct; 80(2):442–57. https://doi.org/10.1016/j.neuron.2013.09.032 PMID: 24139044

51. LaMonica BE, Lui JH, Hansen D V., Kriegstein AR. Mitotic spindle orientation predicts outer radial glial cell generation in human neocortex. Nature. 2013; 9(4):1665. https://doi.org/10.1038/ncomms2647 PMID: 23575669

52. Gertz CC, Lui JH, LaMonica BE, Wang X, Kriegstein AR. Diverse behaviors of outer radial glia in developing ferret and human cortex. J Neurosci. 2014 Feb; 34(7):2559–70. https://doi.org/10.1523/JNEUROSCI.2645-13.2014 PMID: 24523546

53. Heng X, Guo Q, Leung AW, Li JYH. Analogous mechanism regulating formation of neocortical basal radial glia and cerebellar Bergmann glia. Elife. 2017 May 10; 6:e23253. https://doi.org/10.7554/eLife.23253 PMID: 28489004

54. Stahl R, Walcher T, De Juan Romero C, Pilz GA, Cappello S, Irmler M, et al. Trnp1 regulates expansion and folding of the mammalian cerebral cortex by control of radial glial fate. Cell. 2013 Apr 25; 153(3):535–49. https://doi.org/10.1016/j.cell.2013.03.027 PMID: 23622239

55. Mori T, Tanaka K, Buffo A, Wurst W, Kuhn R, and Gotz M. Inducible Gene Deletion in Astroglia and Radial Glia—A Valuable Tool for Functional and Lineage Analysis. Glia. 2006;(54):21–34. https://doi.org/10.1002/glia.20350 PMID: 16652340

56. Sillitoe R, Joyner A. Morphology, molecular codes, and circuitry produce the three-dimensional complexity of the cerebellum. Annu Rev Cell Dev Biol. 2007; 23:549–77. https://doi.org/10.1146/annurev.cellbio.23.090506.123237 PMID: 17506688

57. Louvi A, Alexandre P, Métin C, Wurst W, Wassef M. The isthmic neuroepithelium is essential for cerebellar midline fusion. Development. 2003; 130(22):5319–30. https://doi.org/10.1242/dev.00736 PMID: 14507778

58. Figueres-Oñate M, García-Marqués J, López-Mascaraque L. UbC-StarTrack, a clonal method to target the entire progeny of individual progenitors. Sci Rep. 2016; 6(1):33896. https://doi.org/10.1038/srep33896 PMID: 27654510

59. Schneider CA, Rasband WS, Eliceiri KW. NIH Image to ImageJ: 25 years of image analysis. Nat Methods. 2012 Jun 28; 9:671. PMID: 22930834

60. Fiala JC. Reconstruct: A free editor for serial section microscopy. J Microsc. 2005; 218(1):52–61.

61. Leto K, Arancillo M, Becker EBE, Buffo A, Chiang C, Ding B, et al. Consensus Paper: Cerebellar Development. Cerebellum. 2016 Dec; 15(6):789–828 https://doi.org/10.1007/s12311-015-0724-2 PMID: 26439486

62. Golden JA, Fields-Berry SC, Cepko CL. Construction and characterization of a highly complex retroviral library for lineage analysis. Proc Natl Acad Sci U S A. 1995; 92(12):5704–8. PMID: 7777573

63. Fuentealba LC, Rompani SB, Parraguez JI, Obernier K, Romero R, Cepko CL, et al. Embryonic Origin of Postnatal Neural Stem Cells. Cell. 2015; 161(7):1644–55. https://doi.org/10.1016/j.cell.2015.05.041 PMID: 26091041

64. Estivill-Castro V. Why So Many Clustering Algorithms: A Position Paper. SIGKDD Explor Newsl. 2002; 4(1):65–75. https://doi.org/10.1145/568574.568575

65. Walsh C, Cepko CL. Widespread dispersion of neuronal clones across functional regions of the cerebral cortex. Science. 1992 Jan; 255(5043):434–40. PMID: 1734520

66. Kirkwood TB, Price J, Grove EA. The dispersion of neuronal clones across the cerebral cortex. Science. 1992; 258(5080):317–20. PMID: 1411530

67. Figueres-Oñate M, García-Marqués J, Pedraza M, De Carlos JA, López-Mascaraque L. Spatiotemporal analyses of neural lineages after embryonic and postnatal progenitor targeting combining different reporters. Front Neurosci. 2015 Mar 17; 9:87 https://doi.org/10.3389/fnins.2015.00087 PMID: 25852461

68. Calzolari F, Michel J, Baumgart EV, Theis F, Götz M, Ninkovic J, et al. Fast clonal expansion and limited neural stem cell self-renewal in the adult subependymal zone. Nat Neurosci. 2015; 18(4):490–2. https://doi.org/10.1038/nn.3963 PMID: 25730673

69. Kamei Y, Inagaki N, Nishizawa M, Tsutsumi O, Taketani Y IM. Visualization of mitotic radial glial lineage cells in the developing rat brain by Cdc2 kinase-phosphorylated vimentin. Glia. 1998; 23:191–9. PMID: 9633804

70. Gillespie DT. A general method for numerically simulating the stochastic time evolution of coupled chemical reactions. J Comput Phys. 1976; 22(4):403–34. https://doi.org/10.1016/0021-9991(76)90041-3

71. Sandmann W. Discrete-time stochastic modeling and simulation of biochemical networks. Comput Biol Chem. 2008 Aug; 32(4):292–7. https://doi.org/10.1016/j.compbiolchem.2008.03.018 PMID: 18499525

72. R Foundation for Statistical Computing. R: A Language and Environment for Statistical Computing. Vienna, Austria; 2018. https://www.r-project.org/

73. Carletti B, Grimaldi P, Magrassi L, Rossi F. Specification of cerebellar progenitors after heterotopic-heterochronic transplantation to the embryonic CNS in vivo and in vitro. J Neurosci. 2002; 22(16):7132–46. https://doi.org/10.1523/JNEUROSCI.22-16-07132.2002 PMID: 12177209

74. Weyer A, Schilling K. Developmental and cell type-specific expression of the neuronal marker NeuN in the murine cerebellum. J Neurosci Res. 2003 Aug; 73(3):400–9. https://doi.org/10.1002/jnr.10655 PMID: 12868073

75. Leto K, Carletti B, Williams IM, Magrassi L, Rossi F. Different types of cerebellar GABAergic interneurons originate from a common pool of multipotent progenitor cells. J Neurosci. 2006 Nov 8; 26(45):11682–94. https://doi.org/10.1523/JNEUROSCI.3656-06.2006 PMID: 17093090

76. Mecklenburg N, Martinez-Lopez JE, Moreno-Bravo JA, Perez-Balaguer A, Puelles E, Martinez S. Growth and differentiation factor 10 (Gdf10) is involved in Bergmann glial cell development under Shh regulation. Glia. 2014 Oct; 62(10):1713–23. https://doi.org/10.1002/glia.22710 PMID: 24963847